Excitation dynamics in single molecular crystals of α-hexathiophene from femtoseconds to milliseconds

S. V. Frolov, Ch. Kloc, and B. Batlogg
Bell Laboratories, Lucent Technologies, 600 Mountain Avenue, Murray Hill, New Jersey 07974

M. Wohlgenannt, X. Jiang, and Z. V. Vardeny
Physics Department, University of Utah, Salt Lake City, Utah 84112
(Received 31 August 2000; published 19 April 2001)

We identify odd- and even-parity states and measure transient photomodulation spectra of Frenkel excitons in α-hexathiophene single crystals. The lowest Frenkel excitons are characterized by a stimulated emission band at ~2 eV and an absorption band at 1.3 eV. Intramolecular internal conversion governs transitions from upper excited states to the lowest exciton and occurs in 200 fs. We observe exciton trapping on the nanosecond time scale; as a result, the millisecond photomodulation spectrum is dominated by the absorption of trap states. Using photoinduced-absorption-detected magnetic resonance spectroscopy, we identify the excited-state absorption spectra of triplet excitons and polarons, both of which are produced with a low quantum yield. The triplet absorption band is structureless and approximately 4 times wider than the absorption of singlet excitons. The long-lived photoexcitations are also studied by the photoluminescence-detected magnetic resonance (PLDMR) technique, as a function of the magnetic field orientation in the crystal *b*-*c* plane. We find that there exist two triplets with similar zero-field-splitting parameters, but with the principal axes oriented along different directions, giving rise to six magnetic resonances in the PLDMR spectra.

DOI: 10.1103/PhysRevB.63.205203 PACS number(s): 78.47.+p, 78.55.Kz, 78.30.Jw

I. INTRODUCTION

In recent years oligothiophenes and α-hexathiophene (α6T), in particular, have been extensively studied as model π-conjugated molecular systems for potential applications in optoelectronics.[1] Research initially concentrated on thin evaporated films,[2,3] and in recent years its focus has gradually shifted toward single crystals.[4] Although practical devices are likely to be produced from disordered polycrystalline films, it is also necessary to understand the photophysics of pure single crystals. Optical properties of α6T single crystals have been primarily characterized using linear absorption and luminescence spectroscopies.[5] Recently, a time-resolved optical spectroscopy has been applied to this material.[6] Here we present further analysis of photoexcitation dynamics in α6T single crystals using the time-resolved spectroscopy.

Primary photoexcitations in organic molecular crystals are Frenkel excitons,[7,8] i.e., tightly bound electron-hole pairs localized on single molecules. The theory of molecular Frenkel excitons has been developed rather extensively,[9,10] and an enormous amount of experimental work has been accumulated on this topic.[11] Most experimental studies have been focused on doped and low-purity molecular crystals and restricted in the time domain to nanosecond and longer time scales.[12] Exciton dynamics in mixed crystals are obscured by exciton trapping on guest molecules and difficult to observe. High-purity single crystals are therefore required for the analysis of intrinsic dynamics, which includes intra- and intermolecular phonon-assisted relaxation, intermolecular charge transfer, exciton migration, self-localization due to lattice relaxation, radiative recombination, and intersystem crossing.[8] Recently, we have grown a variety of single molecular crystals, in which carrier mobilities at low temperature approach those of the purest inorganic semiconductors.[4,13] Typical carrier trap concentrations[4,13] of less than $10^{15}\,\mathrm{cm}^{-3}$ suggest that exciton trapping on defects in these crystals should be insignificant in the femto- and picosecond time domain. Such materials thus offer a unique opportunity to understand how various electronic processes contribute to the excited-state relaxation.

II. EXPERIMENTAL SETUP

As described elsewhere,[14] α6T single crystals are grown in the form of free-standing platelets with thickness from 1 to 10 μm and sizes up to 1 cm. It has been established that α6T molecules can crystallize in two similar crystallographic phases: the low-temperature (LT) and the high-temperature (HT) phase.[15] Both of these phases have been thoroughly studied[16] and found to be herringbone structures with monoclinic unit cells containing four α6T rigid rodlike molecules. These molecules are aligned parallel to the plane formed by the *a* and *c* crystal axes; the *b* crystal axis is thus almost perpendicular to the α6T molecules (see Fig. 1 inset). Since the crystal growth direction corresponds to the *a* axis, one can readily measure polarized absorption for light polarizations parallel to the *b* and *c* crystal axes, respectively. Polarized absorption spectra are measured using an Ocean Optics fiber-optic spectrometer.

Photoluminescence (PL) spectra are recorded using an Acton Research 0.3 m spectrometer and a Si photodiode. Measurements of integrated PL intensity in combination with a *Z*-scan technique are used to obtain two-photon absorption spectra. The PL due to two-photon excitation is measured from a thin α6T crystal, while it is translated in and out of the focus of a 100 fs pulsed laser beam having the photon energy below the one-photon absorption edge. The PL inten-

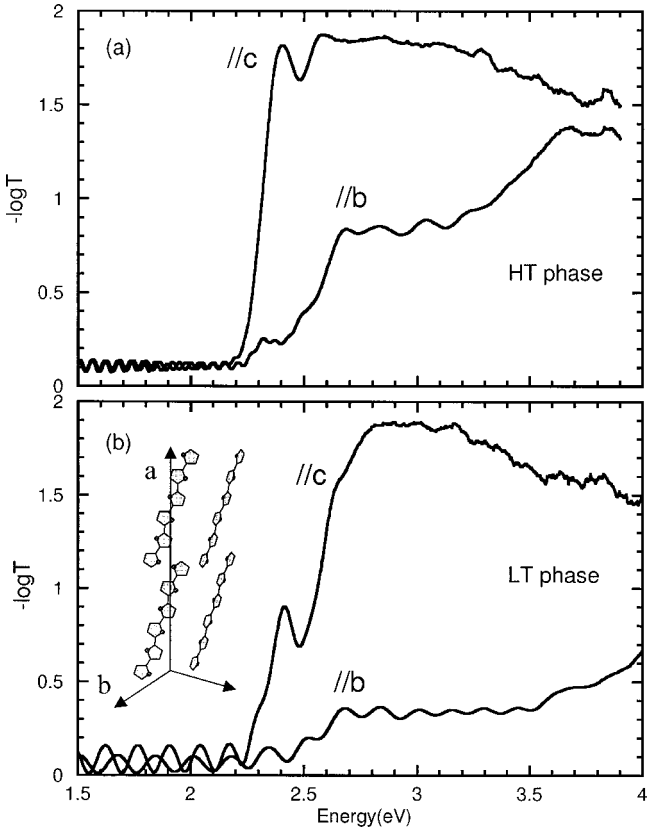

FIG. 1. Polarized absorbance spectra of the HT (a) and LT (b) single crystals for light polarizations parallel to the *b* and *c* crystal axes. The absorbance is not corrected for the reflectivity. The inset schematically shows the crystal unit cell.

sity normalized to the laser peak power and the focal spot size is a measure of the relative two-photon excitation PL yield. The spectrum of this yield vs the two-photon pump energy corresponds to the two-photon absorption; the validity of this statement is later verified experimentally.

A pump-and-probe correlation technique is used to obtain time-resolved photomodulation (PM) spectra by measuring $\Delta T(t)/T$ vs probe photon energy $\hbar\omega$, where T is the probe transmission, ΔT is the change in T due to the pump pulse, and t is the time delay between the pump and probe pulses. Negative ΔT implies photoinduced absorption (PA), whereas positive ΔT can be due to photobleaching or probe-induced stimulated emission (SE). Two electronically synchronized Ti:sapphire mode-locked lasers (Spectra-Physics ''Tsunami''), one of which pumps an optical parametric oscillator (''Opal''), are used to produce 100 fsec pump and probe pulses. The timing jitter between the Ti:sapphire lasers is $\sim$6 ps; for measurements with subpicosecond resolution we used only one of the Ti:sapphire lasers. The pump $\hbar\omega$ is varied from 2.5 to 3.0 eV; typical photoexcitation densities are below $2\times10^{16}\,\mathrm{cm}^{-3}$. The probe $\hbar\omega$ is varied from 0.7 to 2.3 eV; in addition, a short mid-ir spectral range from 0.15 to 0.18 eV is available via the difference-frequency mixing of the signal and idler beams. All measurements are done at room temperature. During the measurements the samples are held either under flowing dry nitrogen or in air. In either case no sample degradation is observed, which would result in the decrease of the PL and PM signals.

We also apply the continuous-wave (cw) PM technique for measuring long-lived photoexcitations in the micro- and millisecond regimes. Two light beams are employed in cw PM spectroscopy. For the excitation beam we use an Ar^+ laser at 457 nm, where the light beam is modulated with an optical chopper. An incandescent tungsten halogen lamp is used as the probe light. A combination of several diffraction gratings, optical filters, and solid state detectors (silicon, germanium, indium antimonide) is used to span the probe $\hbar\omega$ between 0.5 and 2 eV. The PM spectrum vs $\hbar\omega$ is obtained by dividing the pump-beam-induced changes in the probe beam transmission, $\Delta T(\omega)$, by the probe beam transmission $T(\omega)$, where ΔT is measured by a phase-sensitive technique; in this case the PA or $\Delta\alpha$ ($=\alpha_L\Delta T/T$ in the thick-film limit, where α_L is the absorption at the laser frequency) does not depend on the apparatus wavelength response.

The spin associated with a PA band may be obtained by the PA-detected magnetic resonance (PADMR) technique.[34,35] In PADMR we measure the changes in PA induced by a modulated microwave field (in our experiment 3 GHz, modulated at 660 Hz) in resonance with the Zeeman-split spin sublevels in magnetic field H.[34,35] The microwave resonant absorption leads to small changes δT in T. This δT is proportional to δN, the change in photoexcitation density N that is caused by changes in spin-dependent recombination rates induced by the microwaves. Two types of PADMR spectra are possible:[35] the H-PADMR spectrum, in which δT is measured at a fixed probe wavelength λ as the magnetic field H is scanned, and the λ-PADMR spectrum, in which δT is measured at a constant H, in resonance, while λ is scanned. The PADMR measurements are done at 10 K, and the Ar^+ pump laser is operated at 488 nm. The PL-detected magnetic resonance (PLDMR) technique[17] is also employed, where the magnetic resonances are detected by a change δ(PL) in the emission intensity. This experimental method is otherwise analogous to the PADMR technique.

III. STEADY-STATE ABSORPTION AND EMISSION

Exciton states in a crystal can be classified according to the irreducible representations of a unit cell group.[7] The unit cell group of both LT and HT α6T crystals is C_{2h} and the corresponding representations are a_g, a_u, b_g, and b_u.[1,5] These exciton states are based upon the excited states of a single molecule. The latter states can be similarly classified as A_g, A_u, B_g, and B_u according to the same C_{2h} group, which also happens to be the symmetry group of the α6T single molecule.[1] One-photon transitions are allowed only between different-parity states, i.e., $g\rightarrow u$ (gerade to ungerade). However, while the $a_g\rightarrow b_u$ transition is polarized in the *a-c* crystal plane, the $a_g\rightarrow a_u$ transition is polarized along the *b* axis. Since α6T molecules are oriented almost perpendicular to the *b* axis, the low-energy a_u states should have vanishingly small transition dipole moment to the ground state. Two-photon transitions, on the other hand, can occur only between same-parity states, i.e., $g\rightarrow g$ and $u\rightarrow u$. Thus, the two-photon absorption spectrum is expected to provide information about the a_g and b_g excited states.

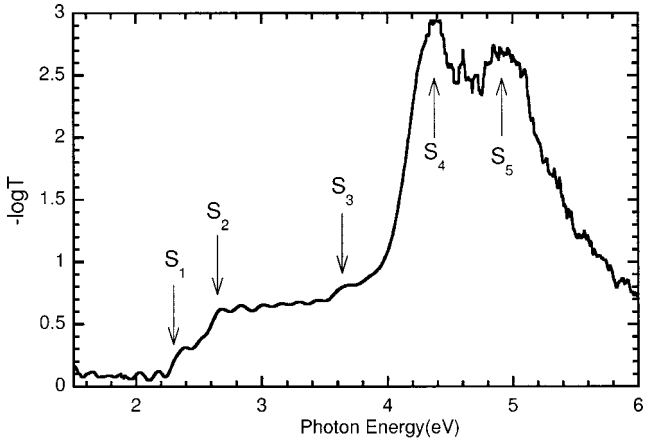

FIG. 2. Unpolarized absorbance spectra of the LT single crystal. Arrows indicate allowed states marked S_1 through S_5.

Figure 1 shows the polarized absorption spectra (uncorrected for the reflectivity) of the two forms of α6T crystal. The oscillations evident at low photon energies are due to the interference fringes, from which we can infer that the HT crystal is about 4 μm thick and the LT crystal is about 1 μm thick. Absorption parallel to the *c* axis could not be reliably measured at $\hbar\omega > 3.0$ eV due to poor optical transmittance. The absorption spectra in Fig. 1 between 2.3 and 3.0 eV can be interpreted in terms of a_u states with weak *b*-polarized and b_u states with strong *ac*-polarized transition dipole moments to the ground state.[5] The origin of *b*-polarized absorption is at $\hbar\omega = 2.3$ eV, whereas the origin of *ac*-polarized absorption is at $\hbar\omega = 2.6$ eV. The energy difference between the two origins of 0.3 eV is the Davidov splitting between the a_u and b_u exciton components of the lowest B_u molecular state. The lowest molecular state $B_u(L)$ is polarized along the long molecular axis (L). This splitting is larger than the strongest Raman-active intramolecular phonon energy (0.19 eV), suggesting that vibronic exciton coupling in the α6T crystals is strong. As a result, some of the vibronic a_u and b_u components are degenerate and therefore intermixed. Consequently, the interpretation of the absorption spectra is quite complicated and requires the introduction of so-called false origins, which are additional optical transitions appearing due to strong electron-phonon coupling.[5]

Absorption measurements at high energies (>3 eV) require very thin crystals. Figure 2 shows the unpolarized absorbance of a thin LT crystal and reveals several higher excited states above 3.6 eV. At least three additional allowed states (either a_u or b_u) at 3.6, 4.4, and 4.9 eV can be distinguished. We speculate that some of these states are based on the $B_u(M)$ molecular state, which is polarized along the short molecular axis (M).[5] A $B_u(M)$ state would explain the appearance of strong *b*-polarized absorption above 4.0 eV, and electronic mixing with this state may also explain the existence of substantial *b*-polarized absorption between 2.6 and 4.0 eV. Traditionally singlet excited states in molecular systems have been marked as $S_0, S_1, \ldots, S_k$ in order of increasing energy, where S_0 is the ground state, S_1 is the first excited state, etc. We adopt this terminology here and mark

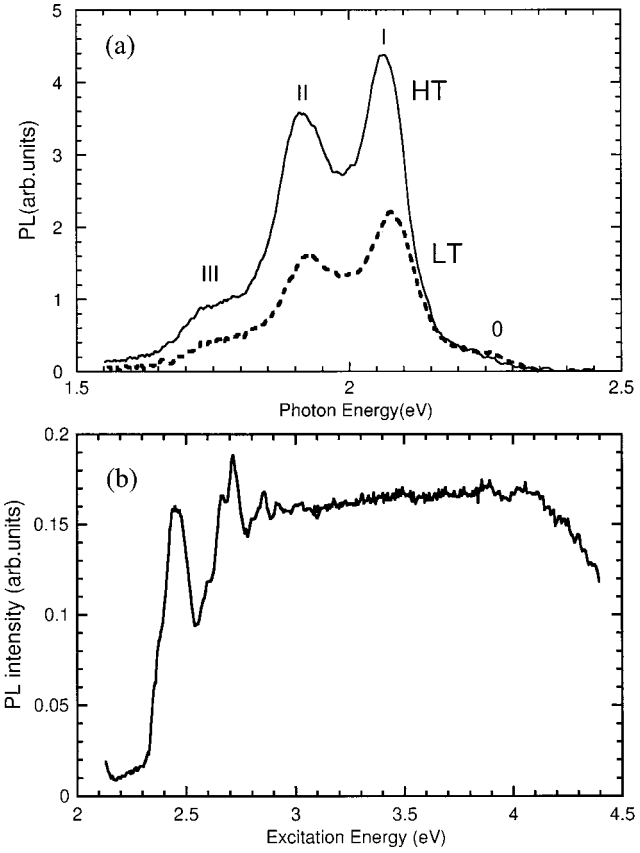

FIG. 3. (a) Emission spectra of the HT (solid line) and LT (dashed line) single crystals; (b) excitation spectrum of photoluminescence in LT single crystals.

all identified states S_1 through S_5 as shown in Fig. 2: S_1 at 2.3, S_2 at 2.6, S_3 at 3.6, S_4 at 4.4, and S_5 at 4.9 eV.

The lowest excited state (S_1) can also be studied by measuring photoluminescence. Figure 3(a) shows the PL spectra of the HT and LT crystals, which were recorded in identical conditions using emission from the front (excited) side of the crystals. Both PL spectra appear to contain vibrational sidebands, which are common in molecular solids and correspond to optical transitions with simultaneous emission of phonons ($0 \rightarrow \nu$, where ν is the number of phonons). However, this vibrationally broadened PL does not obey the Franck-Condon coupling mechanism generally used to describe dipole-allowed transitions.[18] Instead of an expected strong $0 \rightarrow 0$ PL sideband, only a weak shoulder is observed at the origin of one-photon absorption ($\hbar\omega = 2.3$ eV), resulting in a pronounced Stokes shift of the PL spectra with respect to the absorption spectra. This emission is likely due to the a_u exciton (S_1), which indeed has very small dipole coupling with the ground state. Furthermore, PL sidebands I, II, and III in Fig. 3(a) are not equidistant: the separation between bands I and II is 150 meV and between bands II and III 180 meV. This indicates that more than one excited state may contribute to the observed PL. This has been confirmed in several previous studies of α6T films and single crystals,[19] which revealed complex behavior of the PL spectrum at low temperatures and identified several shallow trap states (X traps) and aggregate states.[20] Alternatively, a combination of

several different intramolecular phonon modes can be used to describe uneven S_1 vibronic sidebands. A complete analysis of the PL spectrum in α6T single crystals is currently unavailable.

Two-photon absorption (TPA) can be used to characterize the even-parity a_g and b_g states. To obtain the TPA spectrum, we measure the PL excitation spectrum using two-photon excitation[21] in combination with the *Z*-scan technique. That the PL excitation spectrum corresponds to the TPA spectrum immediately follows from Vavilov-Kasha's rule. The majority of molecular systems obey Vavilov-Kasha's rule, which says that luminescence should occur from the lowest excited state and hence its yield is independent of the excitation energy.[18] Indeed, we find that the PL one-photon excitation spectrum in α6T crystals is practically flat between $\hbar\omega = 2.4$ and 3.2 eV, as shown in Fig. 3(b). Since typical radiative decay rates for allowed singlet states are on the order of $(10\ \text{ns})^{-1}$, it is easy to see that Vavilov-Kasha's rule is a direct consequence of ultrafast relaxation from higher excited states to the lowest (the ultrafast relaxation is discussed in detail below).

In order to measure the two-photon excitation spectra, we use 100 fs pulses with photon energies varying from 1.1 to 1.8 eV. The laser pump beam is focused onto the crystal, which is translated across the focal point. While the sample is translated, the emission rising from two-photon excitation is collected and measured using a silicon detector and a short-pass filter at 650 nm. Figure 4(a) shows a typical result of such *Z*-scan measurements, i.e., the PL intensity (I_e) dependence on the sample coordinate *z*. We model this dependence assuming a Gaussian beam and using the expression $I_e(z) \propto \{P/[1+(\lambda z/\pi w^2)^2]\}^2$, where P is the excitation power, λ is the excitation wavelength, and $2w$ is the excitation beam waist at the focus. Figure 4(a) inset shows that indeed the peak PL intensity grows quadratically with the excitation power. In our measurements we vary the excitation energy, while keeping a constant bandwidth ($\sim$10 nm), and use the ratio $I_e(0)w^2/P^2$ as a relative measure of two-photon absorption.

The resulting TPA spectrum shown in Fig. 4(b) reveals a smooth rise in two-photon absorption coefficient with features similar to those in Figs. 1 and 2, which correspond to allowed $S_1(a_u)$ and $S_2(b_u)$ states at 2.3 and 2.6 eV, respectively. As a result of negligible dipole-dipole interactions between α6T molecules along the *a* crystal axis,[1] the a_g and b_g components of the $1B_u$ molecular state are nearly degenerate with its a_u and b_u components, respectively. Thus TPA can take place at 2.3 and 2.6 eV due to possible intermixing among A_g, A_u, B_g, and B_u single molecule states. The onset of TPA at 3.6 eV, on the other hand, has a relatively weak counterpart at 3.6 eV in the one-photon absorption spectra (S_3). We suggest that the TPA rise at 3.6 eV is due to the nearly degenerate a_g, a_u, b_g, b_u components of an A_g molecular state; the corresponding Davidov splitting is expected to be small because of the negligible dipole-dipole interactions in this state (Davidov splitting is much smaller for even- than for odd-parity states[7]). This conclusion is also supported by the measurements of transient absorption, which are discussed next.

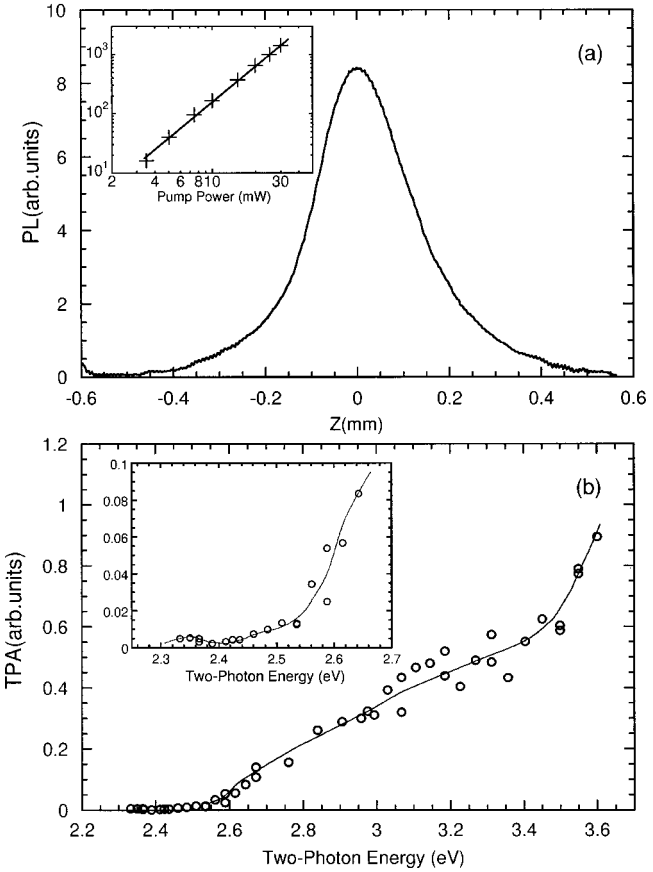

FIG. 4. (a) *Z*-scan measurement of two-photon excited PL in a single crystal; the inset shows the dependence of peak PL intensity vs the excitation power. (b) Two-photon PL excitation spectrum of the HT single crystal; the inset shows the spectrum at low photon energies.

IV. TRANSIENT PHOTOMODULATION

A. Femtosecond and picosecond photomodulation

In order to investigate the relaxation dynamics of excited states in α6T crystals, we measure their transient PM spectra, as shown in Fig. 5 for $t = 5$ ps. The crystals are excited at 2.58 eV with the pump and probe polarizations parallel to the *c* axis. The resultant picosecond PM spectra are dramatically different from those previously measured in thin polycrystalline α6T films.[22,23] First, a pronounced short-lived PA band (band *A*) is observed at $\hbar\omega = 1.25$ eV in the LT crystal and at $\hbar\omega = 1.3$ eV in the HT crystal phase. This band is usually not observed in polycrystalline films. In a recent study of various hexathiophene thin films,[24] a PA band at $\hbar\omega = 1.3$ eV was also observed, but associated with disordered or amorphous parts of the films. Such an assignment in the case of ultrapure crystals is highly unlikely. Second, at $\hbar\omega > 1.85$ eV there is a relatively weaker SE band due to radiative transition from the a_u exciton to the ground state. In this spectral range the probe pulse experiences net optical gain (positive ΔT), the spectrum of which closely matches the PL spectrum. Figure 5(b) inset compares the SE spectrum of the HT α6T crystal with the corresponding PL spectrum (the SE spectrum is arbitrarily offset to compensate for the transient

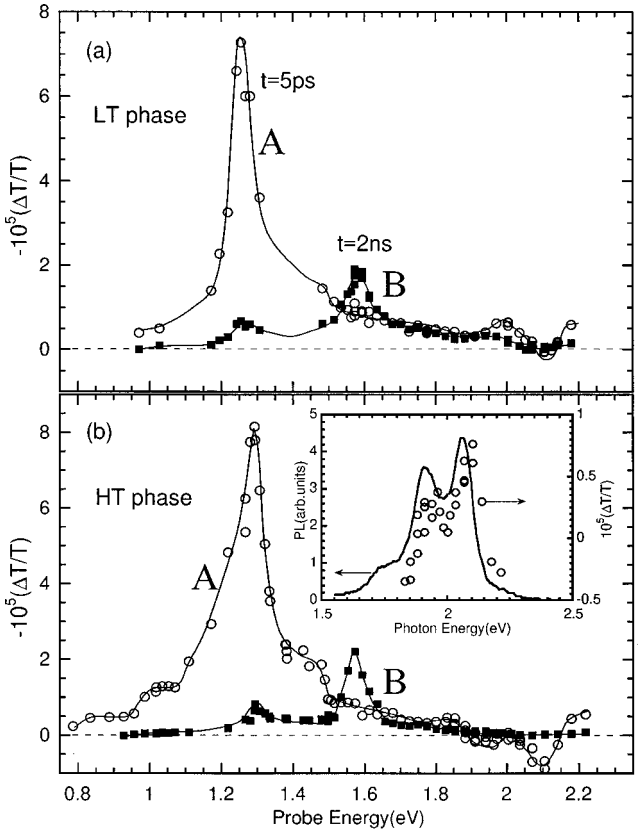

FIG. 5. Transient PM spectra in the LT (a) and HT (b) single crystals at $t=5$ ps (circles) and 2 ns (solid squares). The inset compares the SE spectrum with the PL spectrum of the HT crystal.

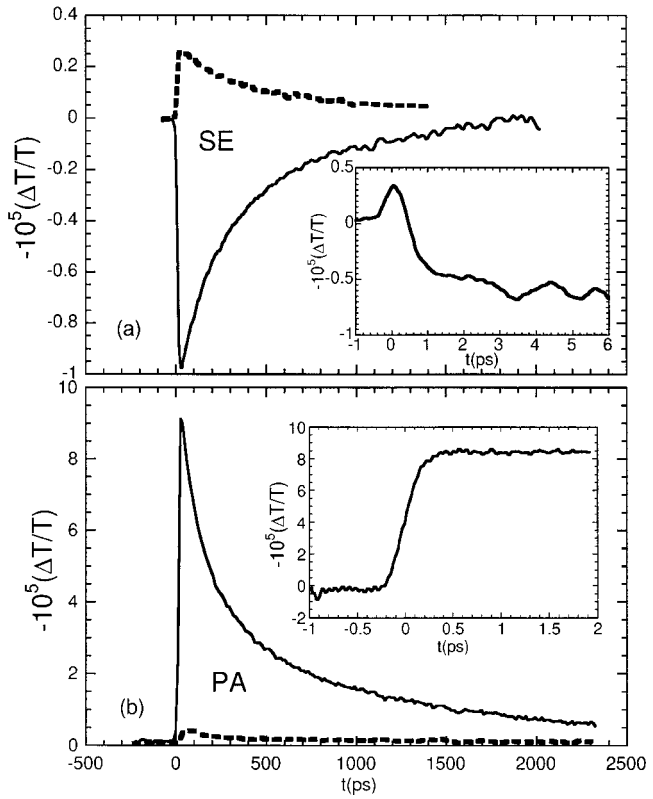

FIG. 6. (a) $\Delta T/T$ decay at $\hbar\omega=2.1$ eV for probe polarization parallel to c (solid line) and to b (dashed line); the inset shows the SE rise time ($\|c$). (b) $\Delta T/T$ decay at $\hbar\omega=1.3$ eV for probe polarization parallel to c (solid line) and to b (dashed line); the inset shows the PA rise time ($\|c$).

PA contribution) and shows that SE and PL share a common origin, i.e., the S_1 exciton at $\hbar\omega=2.3$ eV. Transient SE occurs simultaneously with PA which lowers the net gain experienced by the probe; this is more obvious in the case of the LT crystal, where SE is weaker. From the excitation density and the signal magnitude, we estimate the net optical gain cross section σ_{SE} in the HT crystal to be 2×10^{-18} cm^2. This σ_{SE} is lower than that of luminescent dyes and polymers, such as poly(*p*-phenylene vinylene) derivatives,[25] which can be attributed to the small oscillator strength of the S_1 exciton. SE is c polarized and its decay is well correlated with the PA decay, as shown in Fig. 6(a) (here the PA contribution is evident for the b-polarized probe). Figure 6(b) compares band A decay for probe polarizations parallel to b and c axes and shows that PA at $\hbar\omega=1.3$ eV is also primarily c polarized. Since the picosecond dynamics of SE and PA are well correlated, we can attribute the whole PM spectrum at $t=5$ ps to the S_1 exciton.

Whereas the origin of the vibronically broadened SE band (Fig. 5) in α6T crystals is unambiguous ($S_0\leftarrow S_1$), the origin of the narrow band A is less clear. Since the lowest Frenkel exciton (S_1) is built upon the odd-parity $B_u(L)$ molecular state, we presume that this excitonic state should have a strong transition dipole moment to the higher excited states built upon an even-parity molecular state, nA_g. The even-parity states, in principle, can be identified using TPA spectroscopy. Indeed, Fig. 4(b) shows a broad continuum of states, which have two-photon allowed transitions from the ground state in the spectral range from 2.3 to 3.5 eV; these states are probably responsible for the weak PA observed at $\hbar\omega<1.2$ eV. At $\hbar\omega>3.5$ eV we observe a new onset of TPA, which we attribute to the state S_3 built on the nA_g state. Therefore, band A can be attributed to the optical transition from the a_u exciton (S_1) to the b_g component of the nA_g molecular state (degenerate with S_3). Earlier pump-and-probe measurements on α6T single molecules in solution,[26] which detected a PA band at $\hbar\omega=1.38$ eV, agree with our assignment. The lack of pronounced vibronic sidebands, similar to those in the PL or SE spectra, suggests that the Franck-Condon vibronic overlap factors, which describe the strength of the exciton-phonon coupling, are small for transitions between upper excited states. Therefore, the potential energy surfaces for the S_1 and S_3 states in the configuration coordinate diagram are nearly parallel.

As shown in Fig. 6(b) inset, the PA onset is instantaneous and limited only by the experimental resolution (150 fs), suggesting an ultrafast electronic relaxation from the initially excited state (in the spectral range $\hbar\omega=2.6$–3.2 eV) to S_1. However, the SE onset shown in Fig. 6(a) inset is slower than that of the exciton PA and occurs in about 0.5 ps at excitation energy $\hbar\omega=3.2$ eV. This discrepancy in the PM dynamics at early times can be explained by the competition between the SE ($S_0\leftarrow S_1$) and PA from S_1 to some higher excited state S_i. The potential energy surfaces of S_1 and S_3

states are nearly parallel, i.e., their respective equilibrium configuration coordinates are equal. We speculate that the S_i energy surface is also parallel to the S_1 surface; in this case the PA produced by $S_1 \rightarrow S_i$ and $S_1 \rightarrow S_3$ transitions is insensitive to the exciton thermalization within the S_1 vibronic manifold. On the other hand, the S_0 and S_1 surfaces are not parallel, as evidenced by the Stokes shift between the absorption and PL spectra in Fig. 3(a). Consequently, the SE dynamics due to the $S_0 \leftarrow S_1$ transition should be strongly influenced by the vibronic exciton relaxation within the S_1 manifold. In particular, we expect an ultrafast redshift of the SE spectrum associated with exciton ''cooling,'' which implies that one may observe a relatively slower onset of the optical gain at lower photon energies, corresponding to transitions from the minimum of the S_1 potential surface.

Alternatively, the primary excited states might first decay into the dipole-forbidden a_g state, which then relaxes into the a_u state; however, this is an unlikely scenario, because of the near degeneracy between the a_g and a_u excitons. The ultrafast relaxation to the lowest excited state [in our case the $S_1(a_u)$ exciton] is common for many complex molecular systems.[27] The nonradiative relaxation between molecular states of the same spin multiplicity (singlets in our case) has been termed internal conversion.[16] The rate of internal conversion between two excited states increases exponentially with decreasing difference between the energies of these states.[18] Therefore, internal conversion in single molecules, which contain many closely spaced electronic levels, is the fastest relaxation channel for most excited states, except perhaps the lowest one. This situation appears to be preserved in molecular crystals, where intermolecular interactions are weak and, consequently, their ultrafast dynamics are determined primarily by intramolecular interactions and intramolecular relaxation.

In order to emphasize the importance of internal conversion in organic semiconductors, we directly measure the ultrafast relaxation between different excited states in α6T crystals using a three-beam photomodulation technique.[28] In these measurements [shown schematically in Fig. 7(a)] we use the first excitation pulse ($\hbar\omega = 2.6$ eV) to generate the S_1 excitons, then after vibrational cooling the second excitation pulse ($\hbar\omega = 1.3$ eV) to reexcite these excitons to a higher excited state (S_3). The probe pulse at $\hbar\omega = 1.3$ eV is used to monitor the changes in the sample transmission induced by both pump pulses. Figure 7(b) shows the PA transient signal with only the first pump (broken line) and both pump pulses (solid line). The second pump is delayed with respect to the first by 100 ps. We observe instantaneous transfer of the S_1 excitons to S_3 followed by ultrafast relaxation (within 200 fs) back to S_1. This observation completely agrees with the fact that internal conversion is the dominant relaxation channel in organic semiconductors. This confirms our previous conclusion that the primary relaxation channel from upper excited states, either one- or two-photon allowed, is internal conversion and explains the ultrafast photogeneration of the S_1 excitons. A different behavior would be observed in the case of exciton dissociation and subsequent formation of a charge transfer (CT) state. It has been suggested that the lowest CT state (an analog of a Wannier exciton in inorganic

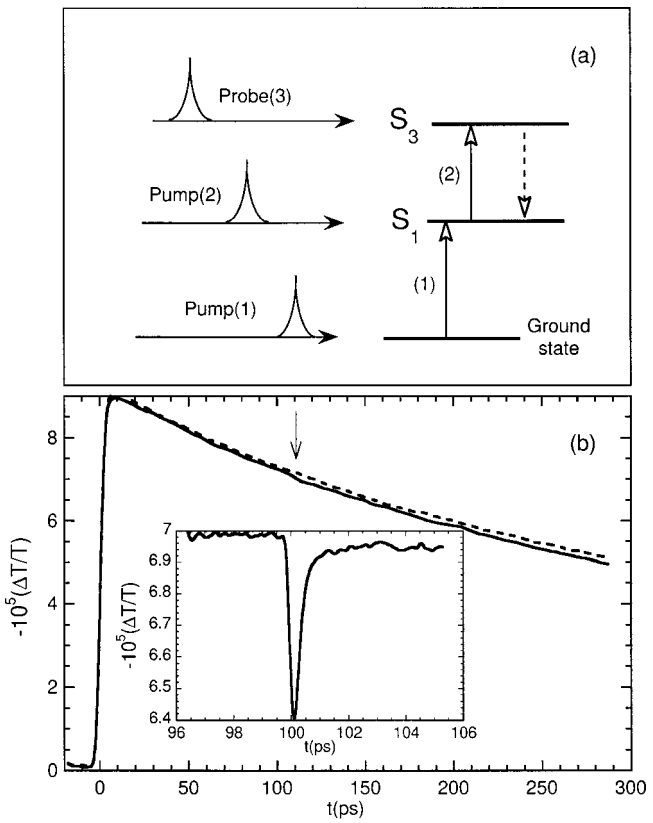

FIG. 7. (a) Three-beam photomodulation diagram. (b) $\Delta T/T$ decay at $\hbar\omega = 1.3$ eV induced by the first pump pulse only (dashed line) and both pump pulses (solid line); the inset shows a closeup of the latter.

semiconductors) in polycrystalline α6T films is located at $E_{CT} \approx 2.7$ eV.[29] Therefore, partial relaxation into a CT state is energetically possible for $\hbar\omega > E_{CT} - E(S_1) \sim 0.4$ eV. The recovery of the lowest excited state after reexcitation at $\hbar\omega = 1.3$ eV is indeed incomplete, as evidenced by the long-lived PA quenching component for $t > 100$ ps in Fig. 7(b). About 10% of S_3 excitons do not relax into S_1 and undergo an alternative relaxation route. Among possible alternatives there are singlet fission and exciton dissociation (autoionization), which lead to the formation of the triplet and CT states, respectively. It is known from the literature[11] that the triplet yield due to hot singlet exciton fission is on the order of 2% in molecular crystals, which cannot explain the 10% yield of the long-lived PA quenching component. Therefore, we suggest that the S_3 exciton is an autoionizing state, which partially overlaps with the continuum of delocalized electron and hole pair states. Some of the ionized CT states have lower energies than S_3 and, therefore, allow partial autoionization before S_3 internally converts into S_1 or S_2. Inefficient charge photogeneration is common for all pure organic semiconductors and can be attributed to the large binding energy of Frenkel excitons and fast internal conversion.[11]

PA and SE transients in Fig. 6 show complex exciton recombination dynamics, which cannot be described with a single exponential decay: these transients can be closely fitted, for instance, using a biexponential decay with time constants of $\tau_1 = 150$ ps and $\tau_2 = 1.2$ ns. Although an accurate

interpretation of these dynamics is difficult, we can make several speculations. First, we argue that because of the low excitation density all recombination processes are monomolecular. Indeed, we found that the observed PM dynamics did not depend on the pump power in our experimental setup (e.g., the bimolecular recombination rate increases with increasing pump power). Second, we presume that exciton dissociation does not occur and neglect the geminate recombination that is typically observed in inorganic semiconductors. Third, in a homogeneous system either monomolecular radiative or nonradiative decay will result in an exponential decay. Therefore, we conclude that our samples behave as a heterogeneous system on the picosecond time scale. Since the samples are highly pure single crystals, we can exclude polycrystallinity, grain boundaries, and impurities as the source of this heterogeneity. However, even in the purest material there is always a small amount of crystalline defects. Presumably, some of these defects may act as deep traps or recombination centers for excitons; other traps may disturb the crystal field only enough to localize the exciton in their vicinity (shallow traps). As a result, the trap-assisted recombination, provided that exciton diffusion is fast enough, would lead to a nonexponential PM decay.

Although exciton localization at shallow traps does not affect the PM spectrum, it can change both radiative and nonradiative exciton recombination rates. Consequently, we tentatively attribute the faster decay component (τ_1) to exciton diffusion and weak localization within the inhomogeneous distribution of shallow trapping centers. Some of these weakly localized excitons can be subsequently released due to thermal fluctuations and continue to migrate through the crystal only to be recaptured by other traps. The longer-lived component (τ_2) is determined by the rates of radiative recombination, direct ground-state internal conversion, and possible deep-trap-assisted recombination. Since the PL quantum yield in α6T crystals is only about 15%,[30] τ_2 represents primarily the nonradiative decay rate, which includes internal conversion and trapping. Other possible nonradiative decay channels are intersystem crossing, in which a singlet exciton is converted into a triplet exciton, singlet fission, where a single singlet exciton splits into two triplet excitons, and bimolecular recombination. The latter includes exciton-exciton annihilation, singlet-triplet quenching, and several other Auger-type processes; none of them are expected to play a major role at low excitation densities. Singlet fission is energetically forbidden, since the relaxed singlet exciton energy is substantially lower than the energy of two triplets.[1] Hot singlet fission can occur in principle, but with only a small yield.[11] The intersystem crossing, on the other hand, is a possible decay channel at low densities and this process is known to occur on the nanosecond time scale. However, we later show that intersystem crossing is not the major relaxation route.

The shape of the PM spectrum does not change significantly from 1 ps to 0.5 ns, which suggests that after the initial rapid relaxation the nature of the excited states does not change on the picosecond time scale. Neither radiative nor nonradiative transitions to the ground state change the shape of the PM spectrum; they only change its magnitude. Intersystem crossing and exciton trapping, on the other hand, affect the PM spectrum in a profoundly different manner. Triplet and singlet excitons in organic materials are known to have different PM spectra.[25] Similarly, trapped excitons may have their distinct PM spectra as well; the PL spectrum of trapped excitons indeed differs from that of free excitons.[19,20] We can loosely classify traps as either shallow (depth less than 0.1 eV) or deep (depth greater than 0.1 eV). The smallest observable energy shift in the PM spectra of Fig. 5 is on the order of 0.1 eV. Accordingly, we expect that shallow trapping does not have an observable effect on the shape of the PM spectra. In contrast, exciton localization at deep traps may have an observable effect, especially when such localization is followed by the exciton dissociation or formation of a different excited state. We therefore conclude that intersystem crossing and deep exciton trapping are not seen on the picosecond time scale. This observation agrees with the previous measurements of low charge trap concentration n_t in our α6T single crystals ($n_t < 10^{15}\,\mathrm{cm}^{-3}$);[4] presumably, the density of exciton traps is equally low.

Previous time-resolved PL measurements at low temperature[20] have revealed a significant difference in spectral dynamics between α6T films and crystals. In particular, excitons in films are quickly captured at deep traps, the PL spectrum of which is very different from that of the a_u excitons. In crystals, where the trap density is low, exciton trapping is slower and primarily limited to shallow traps.[20] Therefore, it is not surprising that the transient PM spectra of α6T crystals dramatically differ from those of α6T films.[22,23] The ultrafast dynamics in films are governed by exciton trapping at numerous defects, most of which act as deep traps. As a result, it is impossible to measure the intrinsic PM spectrum of free Frenkel excitons. On the other hand, pure single crystals have much lower density of traps and thus intrinsic Frenkel excitons can be easily identified. This argument is also supported by the observed differences in the absorption spectra of crystals and films; the latter are usually characterized by substantial inhomogeneous broadening.[1] Furthermore, Frenkel exciton stimulated emission has not been observed in films,[24] which suggest that ultrafast exciton deep trapping indeed occurs in disordered materials.

B. Nanosecond and microsecond photomodulation

The shape of the transient PM spectra in α6T crystals starts to change at $t > 0.5$ ns; the nanosecond PM spectrum in fact resembles the picosecond PM spectrum of thin films (see Fig. 5).[22] The main feature of the nanosecond PM spectra is the pronounced PA band at 1.6 eV (band *B*). Figure 8(a) shows the transient PA at 1.6 eV from 0 to 2 ns for two different probe polarizations. First, it is evident that band *B* is strongly *c* polarized. Second, it is possible to subtract the PA contribution due to the a_u excitons and obtain only the response of the long-lived species, as shown in Fig. 8(b). The rise of band *B* is well correlated with the decay of band *A*, i.e., the a_u exciton decay. It is tempting to assign the formation dynamics of band *B* to excitons being trapped at deep traps. These traps are similar to those found in polycrystalline films; the main difference is their respective concentra-

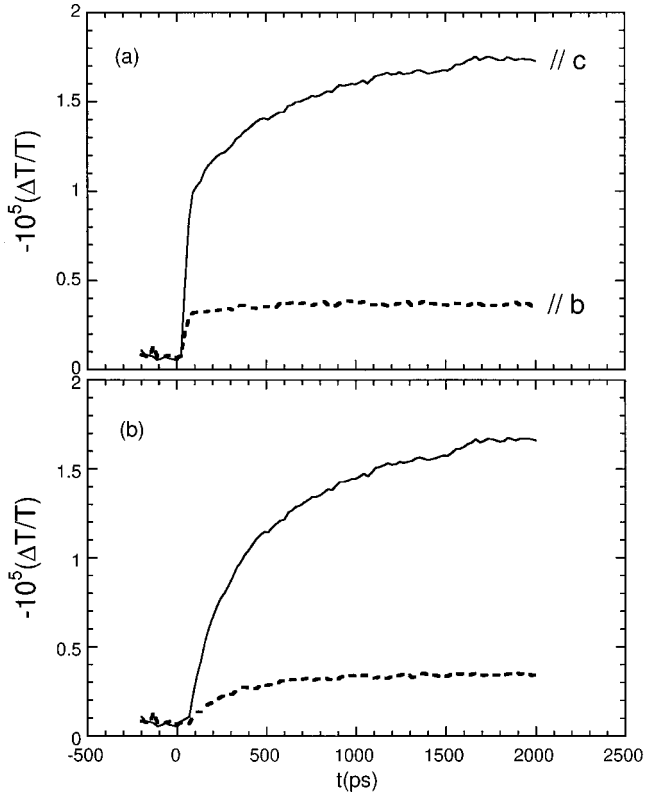

FIG. 8. (a) $\Delta T/T$ decay at $\hbar\omega = 1.6$ eV for probe polarization parallel to *c* (solid line) and to *b* (dashed line); (b) the same decays after subtracting the contribution due to the S_1 decay.

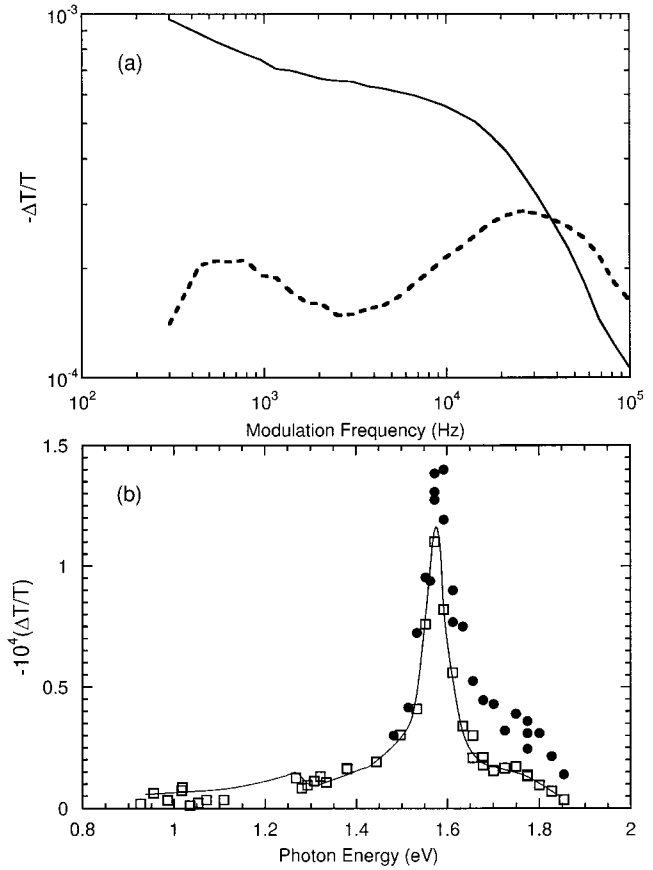

FIG. 9. (a) In-phase (solid line) and quadrature (dashed line) components of the steady-state $\Delta T/T$ signal at $\hbar\omega = 1.6$ eV vs the modulation frequency (f). (b) Steady-state PM spectra at $f = 0.3$ MHz of the HT (solid circles) and LT (squares) single crystals.

tions. Alternative assignments are triplet excitons[23] and charge transfer excitons,[22] both of which have been invoked before to describe the PM spectral dynamics in polycrystalline α6T films.

Triplet excitons have been observed in thin films and discussed in several publications.[31] Their generation with high quantum yield within 1 ps is doubtful, and the measured triplet PA band in films differs substantially from band *B*. Furthermore, our PADMR measurements, which are discussed below, show that the triplet PA band in crystals is also different from band *B*. On this basis, we discard triplet excitons as a possible origin of band *B*. Charge transfer excitons, which have been suggested as an alternative explanation of long-lived PA bands in films, are generally higher in energy than singlet excitons[29] (by about 0.4 eV). Thus their generation in pure crystals is also unlikely.

We therefore assign the long-lived band *B* in crystals to excited states, which were produced as a result of exciton trapping at crystalline defects. The number of defects in evaporated thin films is significantly larger than that in single crystals, which explains the ultrafast formation of long-lived species in films. One of the frequent crystalline defects is a dislocation plane, where neighboring molecules lie parallel to each other and form dimers.[8] These defects are believed to act as both exciton and charge traps and they have been observed in many molecular crystals.[8] Exciton trapping at these sites leads to the formation of so-called predimer states. Since dislocations do not affect the molecular orientation with respect to the crystal axes, one may expect that the PA polarization of a predimer is similar to that of a free exciton. Figure 8 shows that indeed band *B* preserves the polarization of band *A* in the *a*-*c* crystal plane. A complete loss of polarization would have been observed if excitons were trapped at randomly oriented defects or impurities.

Using frequency (f) modulation, we monitor the PA dynamics of trapping states in α6T crystals (both phases) at longer times. Figure 9(a) shows the in-phase and quadrature components of the PA signal from the lock-in amplifier, from which we find that the dynamics are governed by two components with lifetimes of 5 and 260 μs, respectively. The amplitude of the faster component is about 50 times larger than that of the slower one; the slow component may in fact be due to thermomodulation of the crystal's refractive index. The characteristic PA spectrum measured at $f = 0.3$ MHz is shown in Fig. 9(b). The comparison between nano- and microsecond PA spectra shows that, except for the slight spectral narrowing, the PA spectra between $t = 2$ ns and $t \sim 1$ μs do not change significantly. The absence of additional spectral dynamics indicates that a single trapping state is responsible for the exciton trapping in pure crystals.

C. Milisecond photomodulation

In Fig. 10 we show the continuous wave PM spectra of a LT crystal at temperature $\theta = 80$ K. The single crystal,

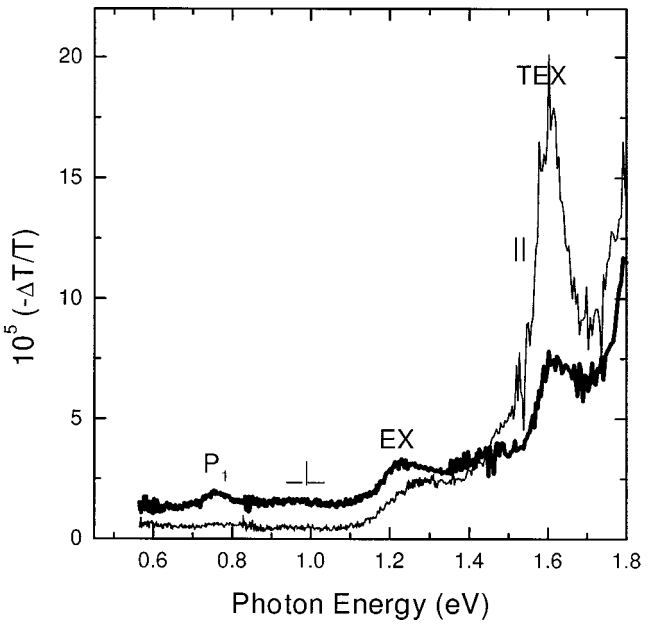

FIG. 10. cw PM spectra of a LT crystal at 80 K, excited at 457 nm and modulated at 660 Hz, with the probe polarization along *c* (solid) and *b* axes (bold).

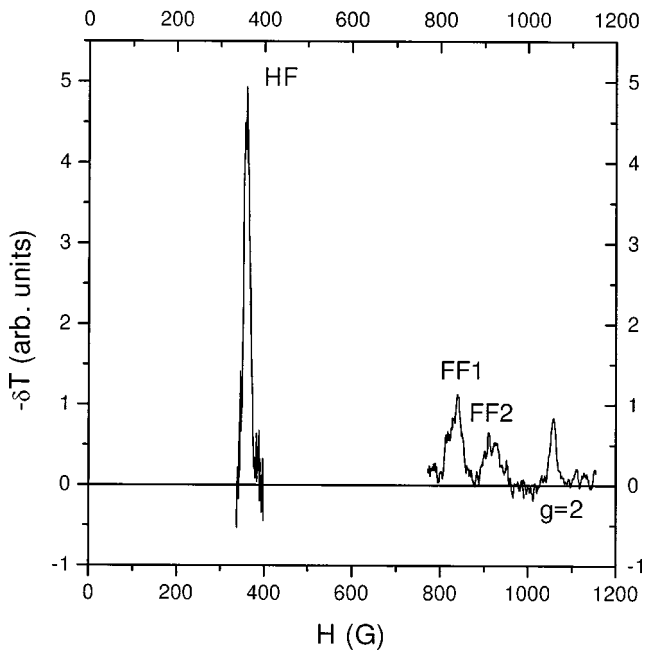

FIG. 11. *H*-PADMR spectrum of a LT crystal; **H** is applied parallel to the *c* axis.

mounted in an optical cryostat, is excited with a cw argon ion laser at 457 nm with the laser light being either *c* polarized (solid line in Fig. 10) or *b* polarized (bold line in Fig. 10). The pump laser beam is modulated with an optical chopper at typically 100 Hz to 1 kHz, which corresponds to the millisecond time domain, if compared to the transient PM measurements. First, we note that the cw PM spectra are quite weak, whereas the cw PL is relatively strong. The PL has to be subtracted from the recorded ΔT signal in order to obtain the PM spectrum. This becomes increasingly difficult at the high-photon-energy part of the spectrum, where the PL contribution dominates. Therefore, we have not been able to isolate the PM spectrum at photon energies $\hbar\omega$ above about 1.8 eV.

The cw PM spectra (Fig. 10) show bands at $\hbar\omega \approx 0.75$ (labeled P_1), 1.25 (EX), and 1.6 eV (TEX). It is seen from a comparison between Figs. 5, 9, and 10 that the cw PA bands EX and TEX resemble the transient PA bands in Figs. 5 and 9. The cw PA spectrum is therefore dominated by the excited states formed following exciton trapping (TEX). The EX band at 1.3 eV can be assigned to the fraction of free excitons left over in shallow traps on the micro- and millisecond time scales probed by the cw PM technique (see also Fig. 9).

V. OPTICALLY DETECTED MAGNETIC RESONANCE

A. PADMR spectroscopy

The PADMR spectroscopic technique measures the *changes* δT of the PA spectrum caused by electron spin resonance of the long-lived photoexcitations. Using this cw technique, we can correlate some PA bands with either spin-1 or spin-$\frac{1}{2}$ excitations. Two types of PADMR spectra are of interest: an *H*-PADMR spectrum, in which a PA band is probed as an applied magnetic field H is scanned; and a λ-PADMR spectrum, in which H is kept in resonance, e.g., with spin $\frac{1}{2}$ or spin 1, while the PA spectrum of the correlated photexcitations is recorded by scanning the probe $\hbar\omega$.

Applying *H*-PADMR spectroscopy to a LT crystal, we find (see Fig. 11) resonances at $H_0 = 1060$ G ($g = 2$, spin-$\frac{1}{2}$ resonance), and quite a strong spin-1 half-field resonance (HF) at 360 G.[30] Additional resonances are also found (labeled FF1 and FF2 in Fig. 11), which belong to the spin-1 full-field pattern. These resonances will be discussed in more detail in connection with PL-detected magnetic resonance below. The half-field resonance is found to be some 160 G below $H_0/2$ or $g = 4$. This is caused by a zero-field-splitting parameter $D \approx 760$ G [$D = \sqrt{(H_0^2 - 4H_1^2)}$].[32] Since D is related to the dipolar interaction between the constituent charges,[33] the triplet exciton wave function extent l may be obtained from it: we conjecture $l = 3.5$ Å, using the relation $l(\mathrm{nm}) = 278/D(\mathrm{G})$.[33]

The spin-$\frac{1}{2}$ λ-PADMR spectrum (Fig. 12, bold) shows resonances at approximately 0.75, 1.3, and 1.6 eV, at positions close to the PA bands P_1, EX, and TEX, respectively (see Fig. 10). The P_1 and TEX PADMR bands are negative, meaning that they are correlated with a resonance-enhanced recombination for spin-$\frac{1}{2}$ photoexcitations. The 1.25 eV band, however, shows an enhancement upon magnetic resonance. These experimental observations can be explained, if we assume that the charged spin-$\frac{1}{2}$ photoexcitations, namely, polarons, may act as quenching sites for the photogenerated excitons. Indeed, nonradiative Auger recombination due to the exciton-polaron interaction has been previously reported in molecular crystals.[11] A resonant reduction of the polaron population (negative resonance at P_1) would then lead to the reduction of the Auger recombination rate, therefore reducing the population of TEX states. At the same time the re-

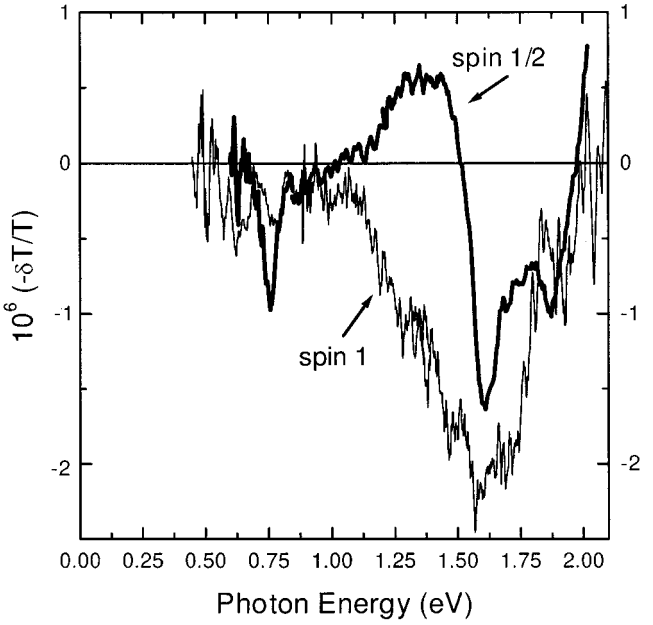

FIG. 12. λ-PADMR spectra of a LT crystal at 10 K of spin 1/2 (bold) and spin-1 (solid) photoexcitations. The laser excitation is at 488 nm, and the microwaves are modulated at 660 Hz.

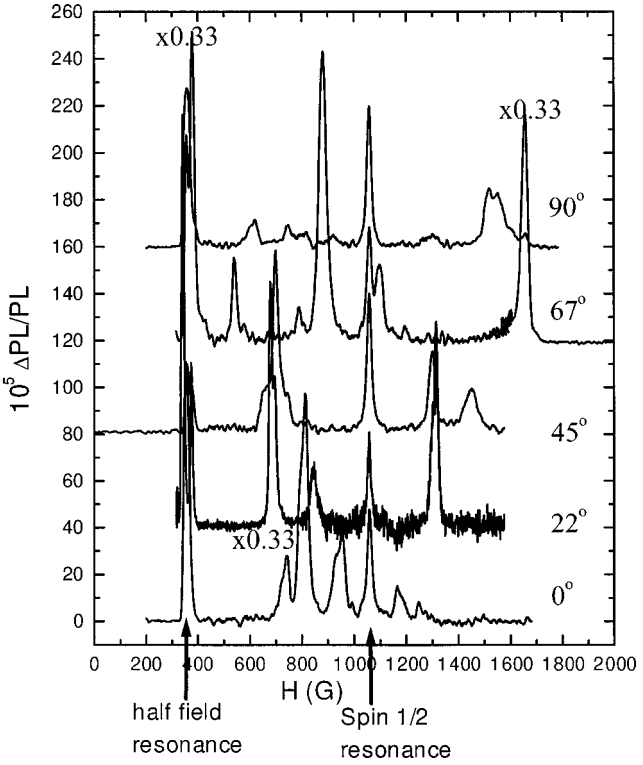

FIG. 13. PLDMR spectra of a LT crystal for different angles between the applied magnetic field H and the crystal c axis, where **H** lies in the b-c plane. 0° denotes **H** parallel to the c axis, whereas 90° denotes **H** parallel to the b axis. The spectra are offset for clarity.

duction of TEX is mirrored by a resonant increase of the free-exciton absorption band, or EX.

As discussed above, a negative resonance is found for the polaron P_1 band. It is well established however, that polarons are correlated to *two* absorption bands,[34] one band (P_1) at photon energies typically around 0.5 eV, whereas the other band (P_2) is in the visible spectral region. Therefore, an alternative interpretation for the PADMR spectrum can be given, where an accidental spectral degeneracy of the high-energy polaron band and P_2 and TEX bands is assumed. Indeed, it was found[35] in disordered films of α6T that the high-energy polaron PA band peaks at ≈1.6 eV. Furthermore, it was found in films of several π-conjugated polymers and oligomers that enhanced recombination of polarons leads to an enhanced bipolaron population.[34] Based on this explanation the PADMR bands at ≈1.6 and 1.25 eV may be interpreted as the spin-$\frac{1}{2}$ resonances of polarons and bipolarons, respectively. Such an assignment is in agreement with the polaron and bipolaron bands obtained by electro-optical measurements in ordered α6T films.[36]

Figure 12 also shows the spin-1 λ-PADMR spectrum (solid line). A comparison between the singlet exciton PA bands (EX and TEX bands, Fig. 6) and the triplet λ-PADMR band (see Fig. 12) shows that the excited-state absorption band of the triplet excitons is approximately four times wider than the singlet excited-state absorption bands. The triplet PA band, as revealed in the λ-PADMR, is very different from the PA band B discussed in Sec. IV B, confirming that band B is not due to triplets.

B. PLDMR spectroscopy

In this section, the complete picture of the magnetic resonances is presented. We measure effects of magnetic resonance on the integrated PL emission strength, where the microwave frequency is at 3 GHz, the magnetic field is swept up to 2000 G, and the microwave intensity is modulated at 660 Hz. Figure 13 shows various H-PLDMR spectra, measured for several orientations of the applied magnetic field in the b-c plane, namely, at angles 0°, 22°, 45°, 67°, and 90°. These angles are understood in the following way: 0° corresponds to the c axis, while 90° corresponds to the b axis. The PLDMR spectra (Fig. 13) show several discrete magnetic resonance lines. The sharp resonance at ≈1060 G is the spin-$\frac{1}{2}$ magnetic resonance and does not change with angle; we therefore conclude that the $g \approx 2$ value is isotropic in the b-c plane. The other resonant lines are assigned to triplets. We note that this is the first time that discrete triplet resonances have been observed in PLDMR of π-conjugated polymers and oligomers to our knowledge. We are able to reproduce the resonant fields (see Fig. 14) for the spin-1 resonances using two effective spin-1 Hamiltonians with different zero-field-splitting tensors, representing the two magnetically inequivalent sites of the monoclinic unit cell. The resonant fields for each triplet are obtained from the following Hamiltonian:

$$H = g\beta \mathbf{H}\cdot\mathbf{S} + D[S_Z^2 - \tfrac{1}{3}S(S+1)] + E(S_X^2 - S_Y^2).$$

Here D and E are two parameters describing the zero-field-splitting tensor in its principal axes. We are able to fit the five spectra within the experimental accuracy assuming that

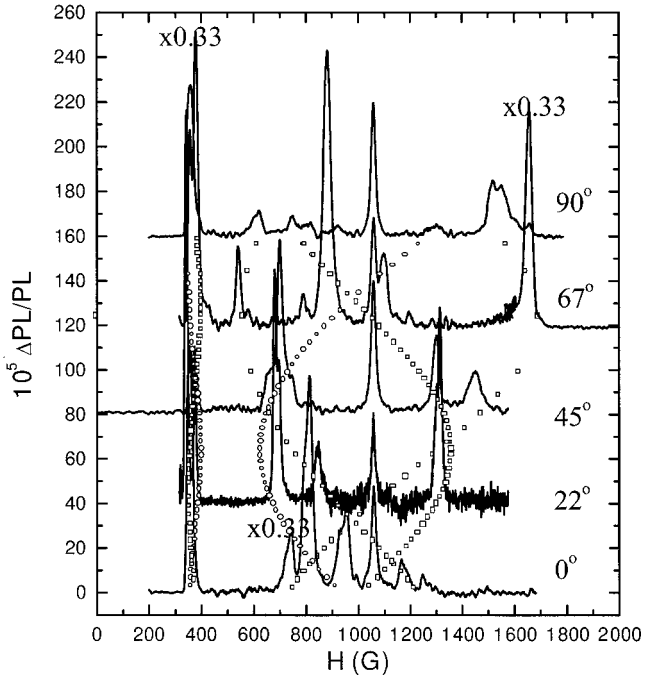

FIG. 14. Experimental spectra of Fig. 13 together with the results (open symbols) of a model calculation for the resonant magnetic fields as a function of the magnetic field orientation in the *b-c* plane.

E parameters of the zero-field-splitting tensors are zero. The triplet excitons associated with the two magnetically inequivalent sites are expected to be similar to each other (we find that their λ-PADMR spectra are identical). The zero-field-splitting parameters *D* are therefore chosen identical for both triplets; the principal axes of the tensors, however, are in general oriented along different directions in space. Five free parameters appear in the Hamiltonians that have been used to model the resonant spin-1 fields as a function of the magnetic field orientation in Fig. 14. These are the *D* value and four additional parameters that determine the orientation of the two zero-field-splitting parameters in space. We find that the resonant fields, within experimental accuracy, are in agreement with an orientation of the tensors along the molecular *N* axes of the two inequivalent sites (see Fig. 14). However, the tensor direction cosines appear in even powers in the Hamiltonian; therefore the sign of these cosines cannot be obtained from the fit, and altogether four principal axis systems lead to the same resonant fields.

VI. SUMMARY

We have measured the transient PM spectra of Frenkel excitons in α6T single crystals and interpreted them in terms of odd- and even-parity states identified by one- and two-photon absorption spectroscopies. The lowest Frenkel excitons are characterized by a vibronically broadened stimulated emission band at ~2 eV and a narrow absorption band at 1.3 eV, which we have used to follow the exciton dynamics. Intramolecular internal conversion governs transitions from upper excited states to the lowest exciton and occurs in 100–200 fs. We have observed exciton trapping on the nanosecond time scale; the secondary excited states produced as a result of exciton trapping have the characteristic absorption band in the photomodulation spectrum. The cw photomodulation spectrum is dominated by excited-state absorption of the trap states; however, we have also observed two additional weak cw bands that we assign to free excitons and charged polarons, respectively. Using spin-1 PADMR spectroscopy, we have identified the excited-state absorption spectrum of triplet excitons, which are produced with a low quantum yield via intersystem crossing. The triplet absorption band is structureless and approximately four times wider than the absorption of singlet excitons. The spin signatures of long-lived photoexcitations have also been studied by the PLDMR technique, as a function of the magnetic field orientation in the crystal *b-c* plane. By employing the PLDMR technique, we have found that there exist two triplets with similar zero-field-splitting parameters, but having the principal axes oriented along different directions giving rise to six magnetic resonances in the PLDMR spectra. These principal axes are oriented along the *N* axes of the molecules at the two magnetically inequivalent sites.

ACKNOWLEDGMENT

The work at the University of Utah was supported in part by the DOE Grant No. DE-FG03-93ER45490.

[1] D. Fichou, *Handbook of oligo- and polythiophenes* (Wiley-VCH, New York, 1999).

[2] F. Garnier, R. Hajlaoui, A. Yassar, and P. Srivastava, Science **265**, 1684 (1994).

[3] A. Dodabalapur, L. Torsi, and H. E. Katz, Science **268**, 270 (1995); A. Dodabalapur, H. E. Katz, L. Torsi, and R. C. Haddon, *ibid.* **269**, 1560 (1995).

[4] J. H. Schön, Ch. Kloc, R. A. Laudise, and B. Batlogg, Appl. Phys. Lett. **73**, 3574 (1998).

[5] M. Muccini, E. Lunedei, A. Bree, G. Horowitz, F. Garnier, and C. Taliani, J. Chem. Phys. **108**, 7327 (1998); M. Muccini, E. Lunedei, D. Beljonne, J. Cornil, J. L. Bredas, and C. Taliani, *ibid.* **109**, 10 513 (1998).

[6] G. Klein, Chem. Phys. Lett. **320**, 65 (2000).

[7] D. P. Craig and S. H. Walmsley, *Excitons in Molecular Crystals* (Benjamin, New York, 1968).

[8] E. A. Silinsh, *Organic Molecular Crystals; Their Electronic States* (Springer-Verlag, New York, 1980).

[9] A. S. Davydov, *Theory of Molecular Excitons* (McGraw-Hill, New York, 1962).

[10] V. M. Agranovich and M. D. Galanin, *Electronic Excitation and Energy Transfer in Condensed Matter* (North-Holland, Amsterdam, 1982).

[11] M. Pope and C. E. Swenberg, *Electronic Processes in Organic*

Crystals and Polymers (Oxford University Press, New York, 1999).

[12] *Spectroscopy and Excitation Dynamics of Condensed Molecular Systems*, edited by V. M. Agranovich and R. M. Hochstrasser (North-Holland, Amsterdam, 1983).

[13] J. H. Schön, S. Berg, Ch. Kloc, and B. Batlogg, Science **287**, 1022 (2000).

[14] Ch. Kloc, P. G. Simpkins, T. Siegrist, and R. A. Laudise, J. Cryst. Growth **182**, 416 (1997).

[15] R. A. Laudise *et al.*, J. Cryst. Growth **152**, 241 (1995).

[16] A. J. Lovinger *et al.*, Macromolecules **29**, 4952 (1996).

[17] L. S. Swanson, J. Shinar, and K. Yoshino Phys. Rev. Lett. **65**, 1140 (1990).

[18] J. B. Birks, *Photophysics of Aromatic Molecules* (Wiley-Interscience, London, 1970).

[19] R. N. Marks, M. Muccini, E. Lunedi, R. Michel, M. Murgia, R. Zamboni, C. Taliani, G. Horowitz, F. Garnier, M. Hopmeier, M. Oestreich, and R. F. Mahrt, Chem. Phys. **227**, 49 (1998).

[20] M. Hopmeier, R. N. Marks, R. Michel, M. Muccini, M. Murgia, R. Zamboni, C. Taliani, G. Horowitz, F. Garnier, M. Oestreich, and R. F. Mahrt, J. Lumin. **76&77**, 416 (1998); R. N. Marks, R. H. Michel, W. Gebauer, R. Zamboni, C. Taliani, R. F. Mahrt, and M. Hopmeier, J. Phys. Chem. B **102**, 7563 (1998).

[21] N. Periasamy, R. Danieli, G. Ruani, R. Zamboni, and C. Taliani, Phys. Rev. Lett. **68**, 919 (1992).

[22] G. Lanzani, S. V. Frolov, P. A. Lane, Z. V. Vardeny, M. Nisoli, and S. DeSilvestri, Phys. Rev. Lett. **79**, 3066 (1997); G. Cerullo, G. Lanzani, M. Muccini, C. Taliani, and S. De Silvestri, *ibid.* **83**, 231 (1999).

[23] K. Watanabe, T. Asahi, H. Fukumura, H. Masuhara, K. Hamano, and T. Kurata, J. Phys. Chem. B **102**, 1182 (1998).

[24] G. Lanzani, G. Gerullo, S. Stagira, S. De Silvestri, and F. Garnier, J. Chem. Phys. **111**, 6474 (1999).

[25] S. V. Frolov, M. Liess, P. A. Lane, W. Gellermann, Z. V. Vardeny, M. Ozaki, and K. Yoshino, Phys. Rev. Lett. **78**, 4285 (1997).

[26] F. Charra, D. Fichou, J.-M. Nunzi, and N. Pfeffer, Chem. Phys. Lett. **192**, 566 (1992).

[27] C. V. Shank, E. P. Ippen, and O. Teschke, Chem. Phys. Lett. **45**, 291 (1977).

[28] S. V. Frolov, Z. Bao, M. Wohlgenannt, and Z. V. Vardeny, Phys. Rev. Lett. **85**, 2196 (2000).

[29] L. M. Blinov, S. P. Palto, G. Ruani, C. Taliani, A. A. Tevosov, S. G. Yudin, and R. Zamboni, Chem. Phys. Lett. **232**, 401 (1995).

[30] The yield is measured using an integrating sphere: M. Wohlgenannt, Z. V. Vardeny, S. V. Frolov, Ch. Kloc, and B. Batlogg, Synth. Met. (to be published).

[31] P. A. Lane *et al.*, Synth. Met. **76**, 57 (1996); X. Wei *et al.*, *ibid.* **84**, 565 (1997).

[32] A. Abragam and B. Bleany, *Electron Paramagnetic Resonance of Transition Ions* (Clarendon, Oxford, 1970).

[33] Z. V. Vardeny and X. Wei, *Handbook of Conducting Polymers*, 2nd ed. (Marcel Dekker, New York, 1998), pp. 639–666, and references therein.

[34] P. A. Lane, X. Wei, and Z. V. Vardeny, Phys. Rev. Lett. **77**, 1544 (1996).

[35] P. A. Lane, M. Liess X. Wei, J. Partee, J. Shinar, A. J. Frank, and Z. V. Vardeny, Chem. Phys. **227**, 57 (1998).

[36] M. G. Harrison, R. H. Friend, F. Garnier, and A. Yassar, Synth. Met. **67**, 215 (1994).